JOURNAL OF GEOPHYSICAL RESEARCH, VOL. 114, A12311, doi:10.1029/2009JA014216, 2009



# Ionospheric response to the corotating interaction region–driven geomagnetic storm of October 2002

D. Pokhotelov,[1,2] C. N. Mitchell,[1] P. T. Jayachandran,[2] J. W. MacDougall,[3] and M. H. Denton[4]

Received 5 March 2009; revised 27 August 2009; accepted 22 September 2009; published 16 December 2009.

[1] Unlike the geomagnetic storms produced by coronal mass ejections (CMEs), the storms generated by corotating interaction regions (CIRs) are not manifested by dramatic enhancements of the ring current. The CIR-driven storms are however capable of producing other phenomena typical for the magnetic storms such as relativistic particle acceleration, enhanced magnetospheric convection and ionospheric heating. This paper examines ionospheric plasma anomalies produced by a CIR-driven storm in the middle- and high-latitude ionosphere with a specific focus on the polar cap region. The moderate magnetic storm which took place on 14–17 October 2002 has been used as an example of the CIR-driven event. Four-dimensional tomographic reconstructions of the ionospheric plasma density using measurements of the total electron content along ray paths of GPS signals allow us to reveal the large-scale structure of storm-induced ionospheric anomalies. The tomographic reconstructions are compared with the data obtained by digital ionosonde located at Eureka station near the geomagnetic north pole. The morphology and dynamics of the observed ionospheric anomalies is compared qualitatively to the ionospheric anomalies produced by major CME-driven storms. It is demonstrated that the CIR-driven storm of October 2002 was able to produce ionospheric anomalies comparable to those produced by CME-driven storms of much greater *Dst* magnitude. This study represents an important step in linking the tomographic GPS reconstructions with the data from ground-based network of digital ionosondes.

**Citation:** Pokhotelov, D., C. N. Mitchell, P. T. Jayachandran, J. W. MacDougall, and M. H. Denton (2009), Ionospheric response to the corotating interaction region–driven geomagnetic storm of October 2002, *J. Geophys. Res.*, *114*, A12311, doi:10.1029/2009JA014216.

## 1. Introduction

[2] Corotating interaction regions (CIRs) created by the interaction between fast and slow solar wind streams are known to cause magnetic storms that are distinct from those produced by coronal mass ejections (CMEs). Unlike the CME-driven disturbances, the CIR-driven storms do not produce a particularly strong ring current and show relatively mild reductions in *Dst* index (typically *Dst* remains above −100 nT). However, the CIR-driven storms can generate other magnetospheric phenomena that are typical for the magnetic storms such as relativistic particle energization and precipitation, ionospheric heating, and enhanced convection [e.g., *Tsurutani et al.*, 2006a]. While the duration of CME-driven storms typically does not exceed tens of hours, the CIR-driven storms can persist for a number of days. Consequently, the energy input into the magnetosphere during CIR-driven events can be comparable to, or even greater than, the energy input during CME-driven events [e.g., *Turner et al.*, 2006].

[3] *Borovsky and Denton* [2006] outlined the main differences between CIR- and CME-driven events and pointed out that CIR-driven storms are characterized by longer periods of the enhanced magnetospheric convection, even though the peak convection speed can be higher for CME-driven events. The enhanced magnetospheric convection is known to be associated with plasmaspheric drainage plumes that are observed in the dayside magnetosphere during both CME- and CIR-driven storms [*Thomsen et al.*, 1998; *Borovsky et al.*, 1998]. Ionospheric anomaly known as the tongue of ionization which spreads from middle to high latitude and over to the polar cap during the main phase of magnetic storms is believed to be linked to the plasmaspheric drainage plumes [*Su et al.*, 2001; *Foster et al.*, 2004]. Formation of the tongue of ionization and the midlatitude ionospheric anomaly (also known as storm enhanced density (SED) anomaly) during major CME-driven storms has been extensively studied using combina-

[1]Department of Electronic and Electrical Engineering, University of Bath, Bath, UK.
[2]Physics Department, University of New Brunswick, Fredericton, New Brunswick, Canada.
[3]Department of Physics and Astronomy, University of Western Ontario, London, Ontario, Canada.
[4]Department of Communication Systems, Lancaster University, Lancaster, UK.


0148-0227/09/2009JA014216$09.00

tions of the data of ionospheric GPS tomography, low Earth orbit (LEO) spacecraft, and incoherent scatter radars [*Foster et al.*, 2005; *Spencer and Mitchell*, 2007; *Pokhotelov et al.*, 2008] as well as numerical modeling [*Sojka et al.*, 1998; *Crowley et al.*, 2006]. Since CIR-driven storms are accompanied by long periods of enhanced convection and ionospheric heating it is reasonable to expect intense ionospheric anomalies such as the SED anomaly and the tongue of ionization to appear. The recent study by *Denton et al.* [2009] using a superposed epoch analysis of data from a single ionosonde during CIR-driven storms reveals clear, repeatable behavior in the midlatitude ionosphere (increase in $h_mF_2$) from the CIR onset for a period of at least 4 days. However, a detailed comparison between the ionospheric anomalies induced by CME- and CIR-driven storms has not been yet performed. This paper will focus on the ionospheric anomalies induced by one of CIR-driven storms at middle and high latitudes and particularly in the polar cap region.

[4] In order to reveal the ionospheric anomalies occurring on a global scale, such as the tongue of ionization and the midlatitude SED anomaly, it is convenient to utilize ionospheric GPS tomography which combines observations of total electron content (TEC) along multiple ray paths of GPS signals received by a network of ground-based GPS receivers. Since the network of GPS receivers is sparse and nonuniform at high latitudes, it is preferable to combine the tomographic reconstructions with other data. In this study the data from one of the Canadian Advanced Digital Ionosondes (CADI) located at Eureka station near the geomagnetic North Pole will be used as an example. We will focus on ionospheric anomalies caused by the CIR-driven storm that occurred during 14–17 October 2002.

[5] Since 2002 the spatial coverage of observational network in the polar cap region has been significantly improved with a number of GPS receivers and digital ionosondes deployed in the Arctic in 2007–2009 as a part of the Canadian High Arctic Ionospheric Network (CHAIN) [*Jayachandran et al.*, 2009]. This study is partly motivated by the intention to analyze polar cap dynamics by assimilating the data from a network of digital ionosondes and the ionospheric GPS tomography.

## 2. CIR-Driven Storm of 14–17 October 2002

[6] The moderate geomagnetic storm which took place on 14–17 October 2002 is used in this study as an example of CIR-driven event. This storm has been identified as CIR-driven by *Zhang et al.* [2007] who analyzed interplanetary and solar conditions for a number of geomagnetic storms that occurred in years 1996–2005. Solar wind data from ACE spacecraft as well as auroral and equatorial geomagnetic indices for the period 13–17 October 2002 are presented in Figure 1. Over this period the solar wind velocity gradually increases from 300 to 600 km/s and the interplanetary magnetic field (IMF) $B_Z$ component shows oscillatory behavior typical for CIR-driven storms which is usually attributed to the effects of interplanetary Alfvén waves [*Tsurutani et al.*, 2006a; *Richardson et al.*, 2006].

[7] As is typical for CIR-driven events this magnetic storm produces only a moderate equatorial signature with the *Dst* index reaching −100 nT at 1400 UT on 14 October 2002 and two less pronounced *Dst* minima occurring on 15 and 16 October. The storm is accompanied by high levels (over 1000 nT) of the auroral electrojet (*AE*) index which are also common for CIR-driven storms [*Tsurutani and Gonzales*, 1987]. Peaks of the *AE* index appear to correlate with the dips of *Dst* index, increases in solar wind density and southward IMF turnings suggesting that the high levels of *AE* are related to the development of the CIR-storm rather than a series of substorm events. This interpretation, particularly on 15–16 October, is also supported by (1) analysis of magnetometer data from GOES spacecraft at geosynchronous orbit where signatures of dipolarizations are largely absent, and (2) energetic particle data from LANL satellites and auroral oval images from Polar EUV which indicate the absence of repeated substorm activity (figures not shown).

## 3. Tomographic Reconstructions

[8] The ionospheric GPS tomography [e.g., *Bust and Mitchell*, 2008] is based on reconstructing an image of the ionospheric plasma from multiple rays of microwave GPS signals. While passing through the dispersive ionosphere the GPS signals suffer a phase advance and a group delay which is proportional to the total electron content (TEC) along the signal path. The TEC is defined as the number of electrons in a column of unit cross-sectional area along the path between a satellite and a receiver. Once values of the slant TEC are known along each signal path, the tomographic inversion can be performed to get a three-dimensional (3-D) distribution of the ionospheric plasma density. Vertical TEC, defined as the number of electrons in a vertical column of unit area, can be derived by integrating through the reconstructed 3-D density distribution.

[9] In this study the 4-D (3-D plus time) inversion algorithm known as Multi-Instrument Data Analysis System [*Mitchell and Spencer*, 2003; *Spencer and Mitchell*, 2007] has been applied to create tomographic images of the ionospheric plasma. A Kalman filter approach is utilized in this algorithm to accommodate temporal changes in the ionospheric plasma density using the statistical Weimer convection model [*Weimer*, 1995] to project the ionospheric images forward in time. TEC data from 51 International GNSS Service (IGS) dual-frequency GPS receivers distributed over the Northern Hemisphere have been used to obtain the ionospheric TEC. Approximate locations of the GPS receivers are shown in Figures 2 and 3 by red labels with four-symbol code indicating the names of IGS stations.

[10] Figure 2 shows distributions of the ionospheric TEC over a large portion of the Northern Hemisphere obtained at 0800 and 0900 UT on 14 October 2002. The color maps indicate the magnitude of vertical TEC (1 TEC unit = $10^{16}$ el/m$^2$). For comparison, the TEC distribution obtained during relatively quiet prestorm day of 13 October 2002 at 0800 UT is shown in Figure 4 (left). Increased TEC values seen during the storm at middle latitudes on the dayside (over Europe and Russia) are believed to be caused partly by the solar radiation and partly by various mechanisms responsible for the formation of the storm enhanced density (SED) anomaly. Such mechanisms may include plasma uplift due to expanded electric convection or thermospheric neutral winds and changes in the ionospheric composition [e.g., *Crowley et al.*,

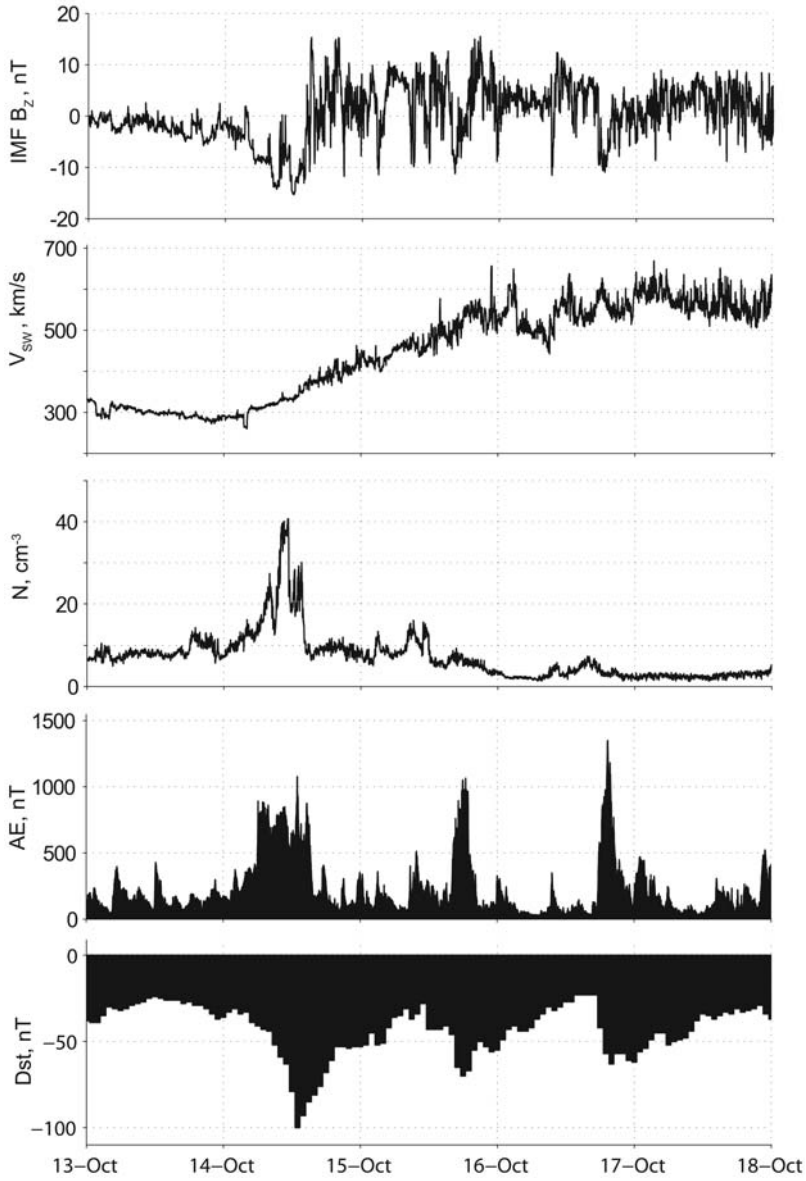


**Figure 1.** Interplanetary magnetic field ($B_Z$ component in GSM coordinates), solar wind velocity and density, auroral electrojet (*AE*) and equatorial electrojet (*Dst*) indices during 14–17 October 2002 magnetic storm.

2006]. Northward of the midlatitude SED anomaly the tongue of ionization is carried antisunward by the ionospheric convection across the polar cap into the night side North American sector. Plot times for Figure 2 were chosen (approximately) when the highest TEC values were observed in the polar cap which happened a few hours before the *Dst* index reaches its minimum on 14 October. Similarly, for large CME-driven storms the highest TEC values in the tongue of ionization are observed few hours prior to the *Dst* minimum [e.g., *Pokhotelov et al.*, 2008].

[11] On 15 October 2002 TEC anomalies at middle and high latitudes also appear prior to the *Dst* minimum though the tongue of ionization is relatively less pronounced (those reconstructions are not presented here). This study will mainly focus on the sequence of tomographic reconstructions for 16 October 2002 which is shown in Figure 3. For comparison, the TEC distribution obtained during quiet prestorm day of 13 October 2002 at 1950 UT is shown in Figure 4 (right). Again, the midlatitude SED anomaly appearing during the storm on the dayside (over the mainland United States of America and southern Canada) is believed to be due to the solar radiation and the above mentioned SED mechanisms. The magnitude of the midlatitude anomaly is substantially higher relative to the 14 October anomaly suggesting that the mechanisms responsible for the SED formations are more intense (see section 5). At 1750 UT (top left plot in Figure 3) we can see the tongue of ionization starting to form over the Hudson Bay area. This moment is manifested by the southward turning of IMF (see Figure 1). Analysis of the Super Dual

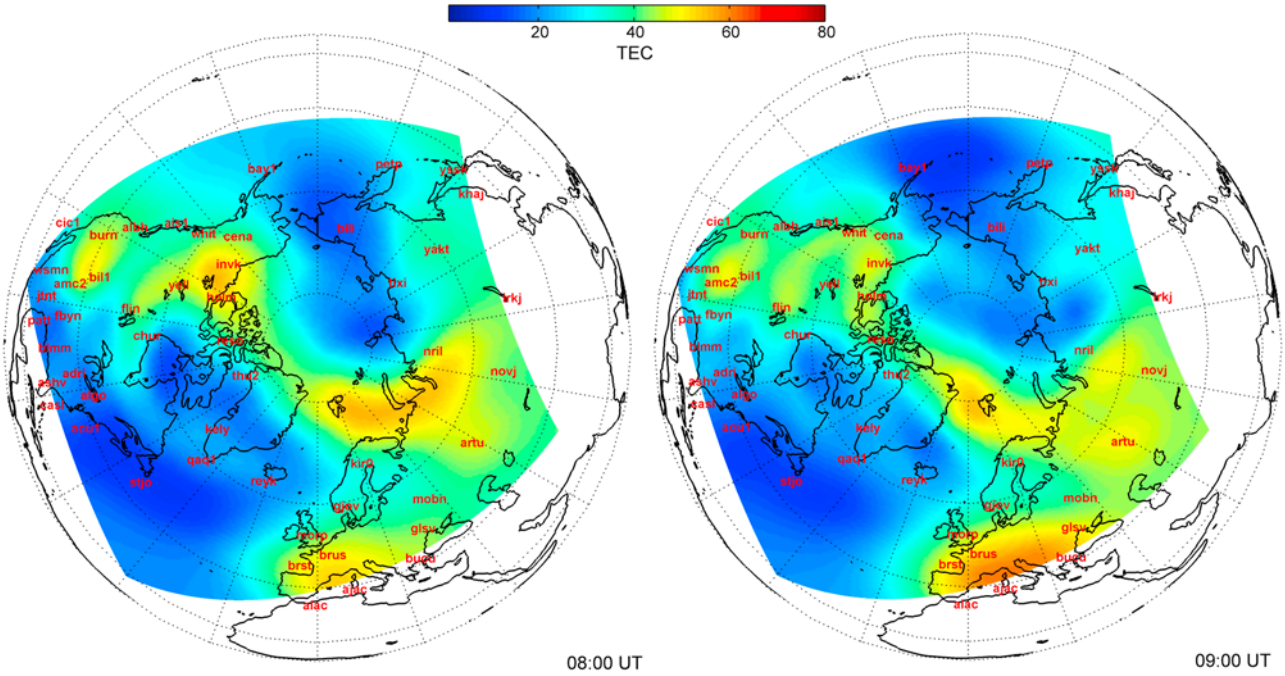


**Figure 2.** Tomographic maps of the ionospheric TEC during 14 October 2002 at 0800 and 0900 UT. Red labels indicate locations of the GPS receivers used for the tomographic reconstructions.

Auroral Radar Network (SuperDARN) convection maps (available at the Johns Hopkins University Applied Physics Laboratory website) for this day shows that the ionospheric convection is globally enhanced after 1740 UT with the cross polar cap potential jumping from 43 to 74 kV between 1730 and 1740 UT. This convection enhancement will be further examined in section 4 using digital ionosonde data. The next tomographic image in Figure 3 taken at 1850 UT (top right plot) shows the tongue of ionization reaching the area of the geomagnetic north pole. At 1950 UT (bottom left plot) the tongue of ionization reaches its peak magnitude and the 2040 UT image (bottom right plot) shows the tongue separating from the midlatitude TEC anomaly with dense plasma patches still drifting antisunward over the northern tip of Greenland.

## 4. Comparison With CADI Data

[12] The Canadian Advanced Digital Ionosondes (CADIs) are able to produce conventional ionograms as well as to derive velocity and direction of the ionospheric drifts from the fixed frequency Doppler measurements with temporal resolution of 30 s [*MacDougall and Jayachandran*, 2001]. Six CADI ionosondes are now deployed (or about to be deployed) in the Canadian Arctic as a part of the CHAIN network. In this study CADI ionosonde data from Eureka station (80°N 274°E) located at Ellesmere Island near the geomagnetic north pole will be used to analyze the ionospheric anomalies revealed by the GPS tomography on 16 October 2002. The location of the Eureka station is indicated by a white cross in Figure 3.

[13] Figure 5 presents a fixed frequency plot for Eureka station showing the virtual height of the *F* layer at the frequency of 4.2 MHz as well as velocity (horizontal and vertical) and azimuth of the ionospheric convection flow. Dashed vertical lines in Figure 5 indicate the moments when four tomographic images shown in Figure 3 were taken. It is clearly seen that the convection changed abruptly around 1740 UT when the velocity jumped from ~250 to 1000 m/s with the convection flow directed northward, i.e., approximately antisunward. This change in the convection corresponds to the moment when the tongue of ionization starts to form according to the GPS tomography (see top left plot in Figure 3).

[14] Fixed frequency CADI plot (Figure 5 (top)) indicates a passage of a few ionospheric inhomogeneities/patches until 1850 UT when the *F* layer becomes dense and uniform. This corresponds to the moment when the tongue of ionization reaches Eureka station as shown by the tomographic image in top right plot of Figure 3. The passage of the uniform and dense tongue of ionization over Eureka at 1950 UT is illustrated by the tomographic image in the bottom left plot of Figure 3. While the tomographic images presented here are merely snapshots, the analysis of animated sequence of images (produced with 10 min resolution) shows uniform flow of dense plasma over the Eureka station between 1850 and 2040 UT. According to the CADI data, the uniform ionospheric tongue passes over Eureka until about 2040 UT when the *F* layer becomes highly inhomogeneous. This corresponds to the moment when the tongue of ionization transforms into large-scale patches separated from the midlatitude TEC anomaly as shown by the tomographic image in the bottom right plot of Figure 3. It has to be pointed out that the 2040 UT tomographic image shown in Figure 3 actually refers to the 10 min time interval centered around 2040 UT, and thus, the reduction of TEC over Eureka seen in the image

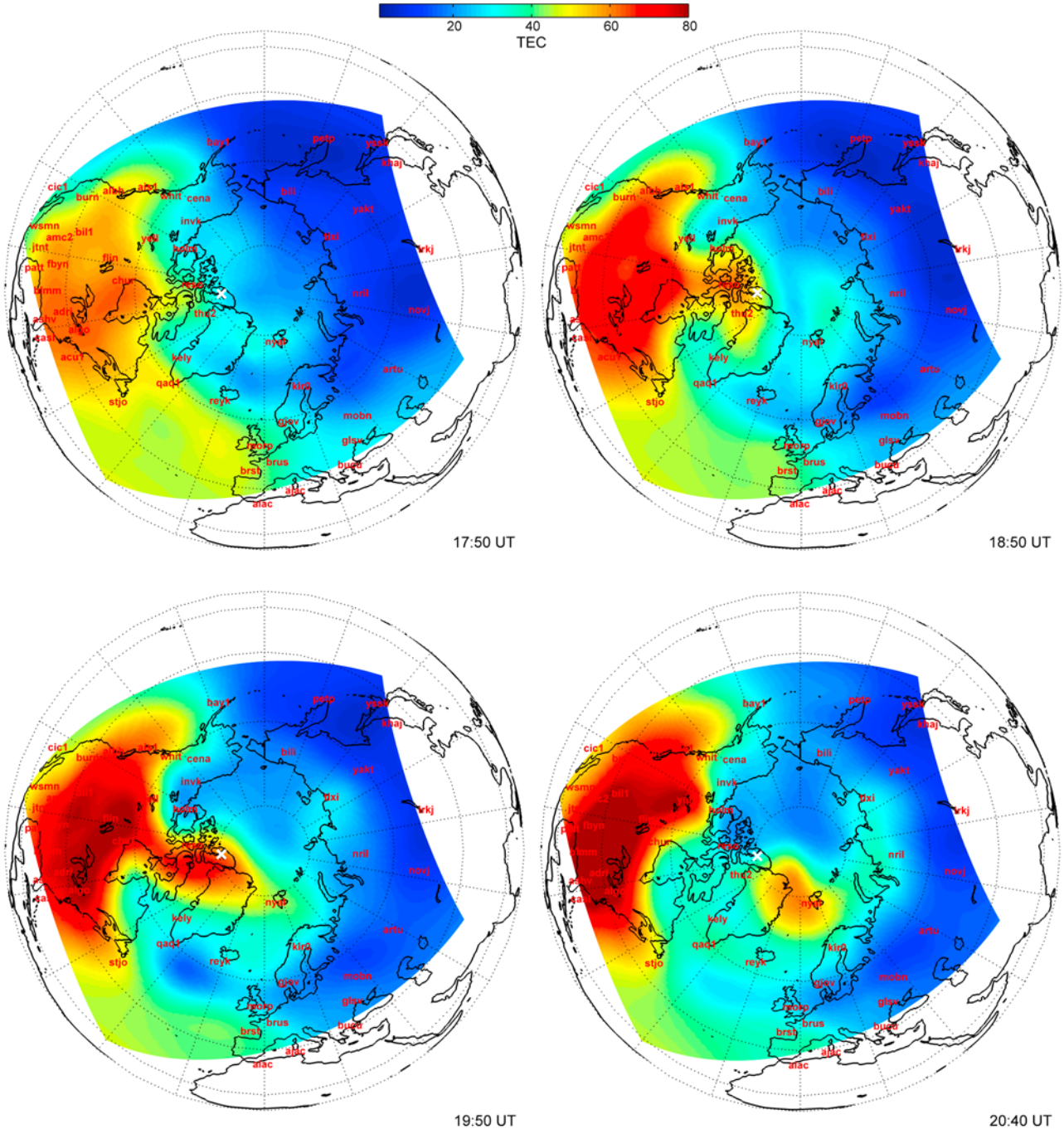


**Figure 3.** Tomographic maps of the ionospheric TEC during 16 October 2002 at (top left) 1750, (top right) 1850, (bottom left) 1950, and (bottom right) 2040 UT. Red labels indicate locations of the GPS receivers used for the tomographic reconstruction. White cross indicates location of the CADI ionosonde at Eureka station.

presumably corresponds to sudden jump in the virtual height seen in the ionosonde data at 2042 UT.

## 5. Discussion

[15] It appears that the CIR-driven magnetic storm of moderate *Dst* magnitude from −100 to −50 nT analyzed above is capable of producing large TEC anomalies (up to 80 TEC units) at middle latitudes and in the polar cap region. For comparison, the tongues of ionization with plasma contents around 100 TEC units are seen in the polar cap during major CME-driven storms with *Dst* magnitudes of ∼−400 nT such as 30 October and 20 November 2003 superstorms. It raises the question whether the *Dst* index can be used as a reasonable measure to predict the intensity of storm-induced ionospheric anomalies without taking into account solar and interplanetary origins of the storm. Obviously, comprehensive analysis of the ionospheric

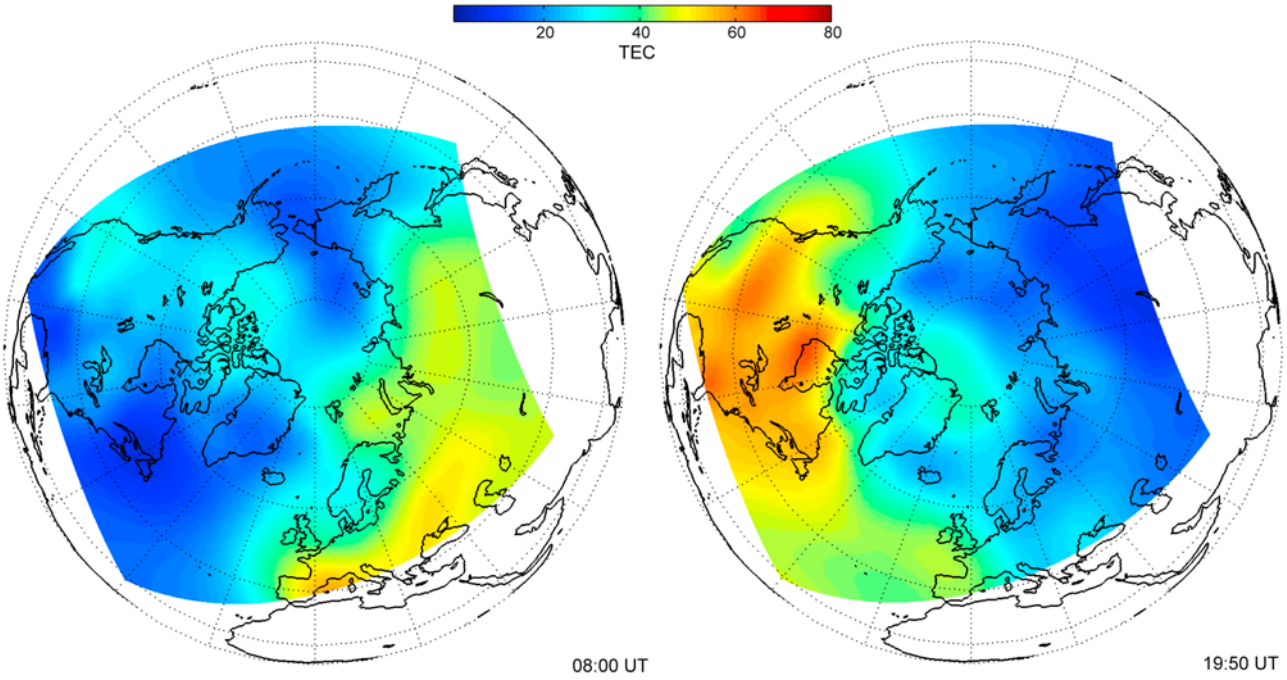


**Figure 4.** Tomographic maps of the ionospheric TEC obtained during relatively quiet prestorm day of 13 October 2002. The tomographic reconstructions at (left) 0800 and (right) 1950 UT.

anomalies observed during other CIR-driven storms is needed to address these issues.

[16] Possible contribution of the plasmaspheric drainage plumes into GPS observations of the tongue of ionization as well as plasmaspheric contribution into the midlatitude SED anomaly remains an open question. Early studies of the plasmaspheric contribution using comparison between GPS-observed TEC values and TEC values derived from radio signals transmitted by Navy Ionospheric Monitoring System (1100 km LEO orbit) spacecraft [*Lunt et al.*, 1999a] as well as ray tracing of the GPS signals through the numerical model of the plasmasphere [*Lunt et al.*, 1999b]

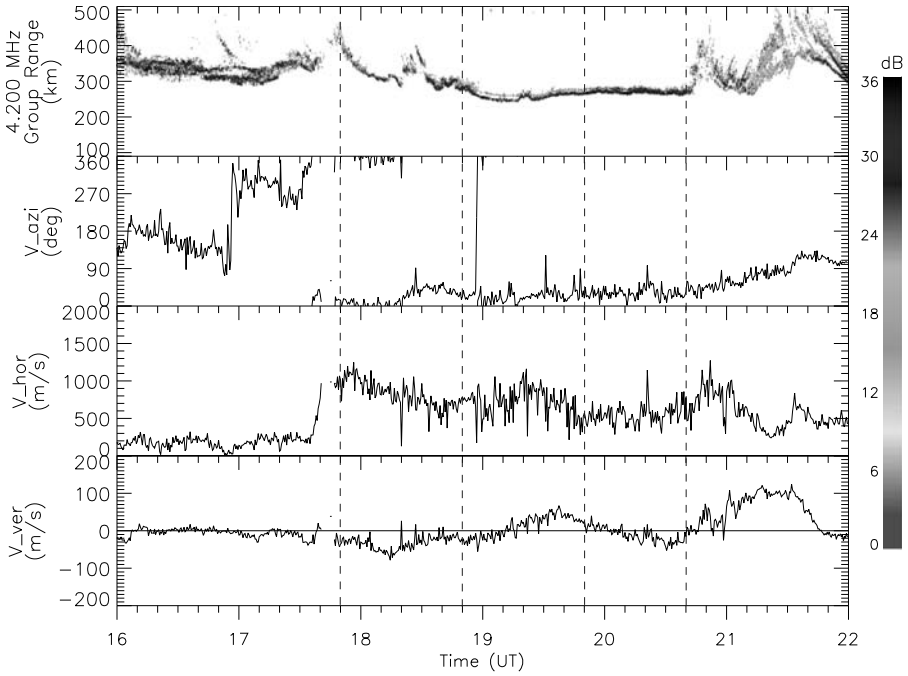


**Figure 5.** CADI ionosonde observations from the Eureka station during 16 October 2002. Top panel shows virtual height of the *F* layer. Three bottom panels show azimuth and two components (horizontal and vertical) of the ionospheric convection flow. Dashed vertical lines indicate time moments corresponding to the tomographic images in Figure 3.

suggested that under quiet geomagnetic conditions the plasmasphere does not contribute more than a few TEC units at middle latitudes. However, data from the upward looking GPS antenna on board the CHAMP spacecraft (~400 km LEO orbit) obtained during 30 October 2003 [*Mannucci et al.*, 2005] and 20 November 2003 [*Yizengaw et al.*, 2006] superstorms suggested that the storm time plasma content above the CHAMP orbit may exceed 20–30 TEC units for middle- and high-latitude regions. Tomographic reconstructions presented in the current paper account for the range of altitudes up to 1600 km, and consequently, GPS observations on LEO orbits higher than the CHAMP orbit are needed to estimate the topside plasma contribution correctly. The upcoming Canadian CASSIOPE/E-POP mission (1500 km apogee LEO orbit) with four upward looking GPS antennas is expected to resolve this problem.

[17] The peak magnitude of TEC anomalies observed during 14–17 October 2002 storm is substantially greater on 16 October compared to 14 October and 15 October even though 16 October has the weakest *Dst* signature. This applies to the anomalies occurring at auroral latitudes and in the polar cap as well as the mid-latitude SED anomaly seen over the US Mainland. A possible explanation is that the ionosphere on 16 October has been preconditioned by the energy deposition (via Joule heating and particle precipitations) during the previous two days of the storm, thus making it easier for the anomalies to form once the ionospheric convection is enhanced on 16 October. Larger TEC magnitudes could also be attributed to the higher values of solar wind speed on 16 October as the solar wind speed exceeds 600 km/s at 1800–2000 UT on 16 October comparing to ~300 km/s at 0800–0900 UT on 14 October. Higher solar wind speed ultimately leads to faster plasma transport across the polar cap, thus giving ionospheric plasma less time to recombine and producing higher TEC values. Corresponding values of the antisunward plasmas convection flow in the polar cap retrieved from the Weimer convection model (used in the tomographic reconstructions presented earlier) are 800–900 m/s at 1800–2000 UT on 16 October and 500–600 m/s at 0800–0900 UT on 14 October. It is worth mentioning that the sharp increase in high-latitude plasma convection around 1740 UT on 16 October (seen in CADI drift data in Figure 5) which triggers the formation of high-latitude anomaly seems to be initiated by the sharp southward turning of IMF at 1720 UT. Presumably, the southward turning of IMF under high solar wind speed conditions facilitates the rapid entry of plasma into the polar cap, thus creating the tongue of ionization. This seems to be consistent with the case described by *Tsurutani et al.* [2006b] for 3 January 2003 CIR-driven event where the high-latitude TEC anomaly is formed in few hours following the sharp CIR-induced southward IMF turning [see *Tsurutani et al.*, 2006b, Figure 8]. A comparative analysis of a number of CIR- and CME-driven storms using some form of the solar wind–magnetosphere coupling function [e.g., *Gonzalez*, 1990] may help to understand the geoeffectiveness of various solar wind parameters (namely, solar wind speed and IMF $B_z$). Such analysis has been recently presented by *Mannucci et al.* [2008] for few major CME-driven storms but has yet to be performed for CIR-driven storms.

[18] The morphology of the TEC anomalies observed in the polar cap during 1400–1700 October 2002 storm resembles the anomalies observed during major CME-driven storms with the SED anomaly appearing at midlatitudes and the tongue of ionization extending into the polar cap. The period over which the tongue of ionization persists as a relatively uniform anomaly spreading from midlatitude to the geomagnetic pole lasts for ~2 h after which the tongue separates from the midlatitude anomaly forming large-scale drifting patches. This is similar to the time scales of the anomalies that are evolving in the polar cap during major CME-driven storms [*Spencer and Mitchell*, 2007; *Pokhotelov et al.*, 2008].

[19] Comparison between the tomographic reconstructions and the measurements of ionospheric convection by the CADI ionosonde in Eureka and SuperDARN radars suggests that the formation of the tongue of ionization on 16 October is triggered by sudden increase in the convection which presumably allows plasma to be transported quickly from midlatitude into the polar cap region. It needs to be pointed out that the tomographic reconstructions presented in this study rely to a certain extent on the Kalman filter technique utilizing the statistical Weimer model as a proxy for the global ionospheric convection. The use of convection data from a network of ionosondes (such as CHAIN) and/or SuperDARN HF radars should improve the quality of reconstructions in the polar cap. The question to which extent the plasma composing the tongue of ionization is transported from lower latitudes or created locally by the enhanced electric fields and/or thermospheric winds is not addressed in this study and needs to be investigated using data assimilation [e.g., *Bust and Crowley*, 2007].

[20] While the comparison between TEC reconstructions and CADI ionosonde observations of the virtual *F* layer height over Eureka shows good qualitative agreement, the question still remains regarding how well the GPS tomography can reproduce the actual values of plasma density at given locations, particularly far away from the nearest ground-based GPS receiver. In order to assess quantitatively the performance of tomographic algorithms, one would have to compare the values of *F* peak plasma density measured by ionosondes with the density values obtained from the tomographic 3-D reconstructions. Such quantitative comparison for the 16 October 2002 event has been performed using CADI observations at Eureka and will be described in details in a separate article (D. Pokhotelov P. T. Jayachandran, C. N. Mitchell, J. W. MacDougall, and M. H. Denton, GPS tomography in the polar cap: comparison with ionosondes and in-situ spacecraft data, submitted to *GPS Solutions*, 2009). In brief summary, vertical density profiles over Eureka station obtained from the tomographic 3-D reconstructions reproduce well the dynamics of the *F* peak density measured by the CADI ionosonde, though the GPS tomography tends to underestimate the *F* peak density by 20–30%. Quantitative comparison of the tomographic reconstructions with in situ spacecraft measurements of cold plasma obtained by the DMSP Special Sensors-Ions, Electrons, and Scintillation thermal plasma analysis instruments

will also be presented by D. Pokhotelov et al. (submitted manuscript, 2009).

## 6. Conclusions

[21] The analysis of ionospheric response to the CIR-driven storm of 14–17 October 2002 suggests that the ionospheric anomalies induced by this storm are comparable to the ionospheric anomalies induced by CME-driven storms of much greater *Dst* magnitude. Tomographic 4-D reconstructions of the ionospheric plasma density using measurements of the total electron content along ray paths of GPS signals reveal the morphology and dynamics of storm-induced plasma anomalies at middle and high latitudes that are similar to the ionospheric anomalies produced by major CME-driven storms with the SED anomaly forming in the dayside midlatitude ionosphere and the tongue of ionization spreading into the polar cap region. Analysis of the CADI ionosonde observations obtained at Eureka station near the geomagnetic north pole shows remarkably good agreement with the dynamics of high-latitude ionospheric anomalies revealed by the GPS tomography with the CADI ionosonde data showing a passage of the tongue of ionization and patches over the Eureka station at the same moments as tomographic images. This outlines potential benefits of intercomparison between the tomographic reconstructions and observations by the network of digital ionosondes (e.g., CHAIN). Quantitative comparison between plasma densities observed by CADI ionosondes and those obtained by the GPS tomography will be presented in a separate article (D. Pokhotelov et al., submitted manuscript, 2009).

[22] **Acknowledgments.** We would like to acknowledge the financial support from the U.K. Science and Technology Facilities Council and the Natural Sciences and Engineering Research Council of Canada. CADI and CHAIN operation is conducted in collaboration with the Canadian Space Agency. We would like to thank the International GNSS Service for making the GPS data available, the University of Kyoto for providing *AE* and *Dst* geomagnetic indices, and the NASA OMNIweb service for providing the solar wind data.

[23] Zuyin Pu thanks Joseph Borovsky and another reviewer for their assistance in evaluating this paper.

## References

Borovsky, J. E., and M. H. Denton (2006), Differences between CME-driven storms and CIR-driven storms, *J. Geophys. Res.*, *111*, A07S08, doi:10.1029/2005JA011447.

Borovsky, J. E., M. F. Thomsen, D. J. McComas, T. E. Cayton, and D. J. Knipp (1998), Magnetospheric dynamics and mass flow during the November 1993 storm, *J. Geophys. Res.*, *103*, 26,373–26,394.

Bust, G. S., and G. Crowley (2007), Tracking of polar cap ionospheric patches using data assimilation, *J. Geophys. Res.*, *112*, A05307, doi:10.1029/2005JA011597.

Bust, G. S., and C. N. Mitchell (2008), History, current state, and future directions of ionospheric imaging, *Rev. Geophys.*, *46*, RG1003, doi:10.1029/2006RG000212.

Crowley, G., et al. (2006), Global thermosphere-ionosphere response to onset of 20 November 2003 magnetic storm, *J. Geophys. Res.*, *111*, A10S18, doi:10.1029/2005JA011518.

Denton, M. H., T. Ulich, and E. Turunen (2009), Modification of midlatitude ionospheric parameters in the F2 layer by persistent high-speed solar wind streams, *Space Weather*, *7*, S04006, doi:10.1029/2008SW000443.

Foster, J. C., A. J. Coster, P. J. Erickson, F. J. Rich, and B. R. Sandel (2004), Stormtime observations of the flux of plasmaspheric ions to the dayside cusp/magnetopause, *Geophys. Res. Lett.*, *31*, L08809, doi:10.1029/2004GL020082.

Foster, J. C., et al. (2005), Multiradar observations of the polar tongue of ionization, *J. Geophys. Res.*, *110*, A09S31, doi:10.1029/2004JA010928.

Gonzalez, W. D. (1990), A unified view of solar-wind magnetosphere coupling functions, *Planet. Space Sci.*, *38*(5), 627–632, doi:10.1016/0032-0633(90)90068-2.

Jayachandran, P. T., et al. (2009), Canadian High Arctic Ionospheric Network (CHAIN), *Radio Sci.*, *44*, RS0A03, doi:10.1029/2008RS004046.

Lunt, N., L. Kersley, G. J. Bishop, and A. J. Mazzella Jr. (1999a), The contribution of the protonosphere to GPS total electron content: Experimental measurements, *Radio Sci.*, *34*(5), 1273–1280.

Lunt, N., L. Kersley, and G. J. Bailey (1999b), The influence of the protonosphere on GPS observations: Model simulations, *Radio Sci.*, *34*(3), 725–732.

MacDougall, J. W., and P. T. Jayachandran (2001), Polar cap convection relationships with solar wind, *Radio Sci.*, *36*(6), 1869–1880.

Mannucci, A. J., B. T. Tsurutani, B. A. Iijima, A. Komjathy, A. Saito, W. D. Gonzalez, F. L. Guarnieri, J. U. Kozyra, and R. Skoug (2005), Dayside global ionospheric response to the major interplanetary events of October 29–30, 2003 "Halloween Storms", *Geophys. Res. Lett.*, *32*, L12S02, doi:10.1029/2004GL021467.

Mannucci, A. J., B. T. Tsurutani, M. A. Abdu, W. D. Gonzalez, A. Komjathy, E. Echer, B. A. Iijima, G. Crowley, and D. Anderson (2008), Superposed epoch analysis of the dayside ionospheric response to four intense geomagnetic storms, *J. Geophys. Res.*, *113*, A00A02, doi:10.1029/2007JA012732.

Mitchell, C. N., and P. S. J. Spencer (2003), A three-dimensional time-dependent algorithm for ionospheric imaging using GPS, *Ann. Geophys.*, *46*, 687–696.

Pokhotelov, D., C. N. Mitchell, P. S. J. Spencer, M. R. Hairston, and R. A. Heelis (2008), Ionospheric storm time dynamics as seen by GPS tomography and in situ spacecraft observations, *J. Geophys. Res.*, *113*, A00A16, doi:10.1029/2008JA013109.

Richardson, I. G., et al. (2006), Major geomagnetic storms ($Dst \leq -100$ nT) generated by corotating interaction regions, *J. Geophys. Res.*, *111*, A07S09, doi:10.1029/2005JA011476.

Sojka, J. J., R. W. Schunk, M. D. Bowline, J. Chen, S. Slinker, J. Fedder, and P. J. Sultan (1998), Ionospheric storm simulations driven by magnetospheric MHD and by empirical models with data comparisons, *J. Geophys. Res.*, *103*, 20,669–20,684.

Spencer, P. S. J., and C. N. Mitchell (2007), Imaging of fast moving electron-density structures in the polar cap, *Ann. Geophys.*, *50*, 427–434.

Su, Y.-J., M. F. Thomsen, J. E. Borovsky, and J. C. Foster (2001), A linkage between polar patches and plasmaspheric drainage plumes, *Geophys. Res. Lett.*, *28*, 111–113.

Thomsen, M. F., J. E. Borovsky, D. J. McComas, R. C. Elphic, and S. Maurice (1998), The magnetospheric response to the CME passage of January 10–11, 1997, as seen at geosynchronous orbit, *Geophys. Res. Lett.*, *25*, 2545–2548.

Tsurutani, B. T., and W. D. Gonzalez (1987), The cause of high intensity long-duration continuous AE activity (HILDCAAs): Interplanetary Alfvén wave trains, *Planet. Space Sci.*, *35*, 405–412.

Tsurutani, B. T., et al. (2006a), Corotating solar wind streams and recurrent geomagnetic activity: A review, *J. Geophys. Res.*, *111*, A07S01, doi:10.1029/2005JA011273.

Tsurutani, B. T., A. J. Mannucci, B. A. Iijima, A. Komjathy, A. Saito, T. Tsuda, O. P. Verkhoglayadova, W. D. Gonzalez, and F. L. Guarnieri (2006b), Dayside ionospheric (GPS) response to corotating solar wind streams, in *Recurrent Magnetic Storms*, *Geophys. Monogr. Ser.*, vol. 167, edited by B. T. Tsurutani et al., p. 245, AGU, Washington, D.C.

Turner, N. E., E. J. Mitchell, D. J. Knipp, and B. A. Emery (2006), Energetics of magnetic storms driven by corotating interaction regions: A study of geoeffectiveness, in *Recurrent Magnetic Storms: Corotating Solar Wind Streams*, *Geophys. Monogr. Ser.*, vol. 167, edited by B. T. Tsurutani et al., p. 113–124, AGU, Washington, D. C.

Weimer, D. R. (1995), Models of high-latitude electric potentials derived with a least error fit of spherical harmonic coefficients, *J. Geophys. Res.*, *100*, 19,595–19,608.

Yizengaw, E., M. B. Moldwin, A. Komjathy, and A. J. Mannucci (2006), Unusual topside ionospheric density response to the November 2003 superstorm, *J. Geophys. Res.*, *111*, A02308, doi:10.1029/2005JA011433.

Zhang, J., et al. (2007), Solar and interplanetary sources of major geomagnetic storms ($Dst \leq 100$ nT) during 1996–2005, *J. Geophys. Res.*, *112*, A10102, doi:10.1029/2007JA012321.

M. H. Denton, Department of Communication Systems, Lancaster University, Lancaster LA1 4WA, UK.

P. T. Jayachandran and D. Pokhotelov, Physics Department, University of New Brunswick, Fredericton, NB E3B 5A3, Canada. (dipo@unb.ca)

J. W. MacDougall, Department of Physics and Astronomy, University of Western Ontario, 1155 Richmond St., London, ON N6A 5B9, Canada.

C. N. Mitchell, Department of Electronic and Electrical Engineering, University of Bath, Bath BA2 7AY, UK.